Journal of Chromatography A, 1503 (2017) 49–56

Contents lists available at ScienceDirect

Journal of Chromatography A

journal homepage: www.elsevier.com/locate/chroma

Effect of cationic monomer content on polyacrylamide copolymers by frit-inlet asymmetrical flow field-flow fractionation/multi-angle light scattering

Hyejin Lee [a], Jin Yong Kim [a], Woonjin Choi [b], Myeong Hee Moon [a,*]

[a] Department of Chemistry, Yonsei University, Seoul, 120-749, South Korea
[b] Kolon Life Science Inc., 13 Kolon-ro, Gwacheon-si, Gyeonggi-do, 427-709, South Korea

ARTICLE INFO

Article history:
Received 16 March 2017
Received in revised form 26 April 2017
Accepted 27 April 2017
Available online 28 April 2017

Keywords:
Cationic polyacrylamide
Cationic monomer content
Field-flow fractionation
Multi-angle light scattering

ABSTRACT

In this study, ultrahigh-molecular-weight (MW) (>10^7 Da) cationic polyacrylamides (C-PAMs), which are water-soluble polymers used in waste water treatment, were characterized using frit-inlet asymmetrical flow field-flow fractionation coupled with multi-angle light scattering and differential refractive detection. C-PAMs copolymerized with acryloxyethyltrimethyl ammonium chloride (DAC) were prepared by varying the feed amount of cationic monomer, polymerization method (solution vs. emulsion), and degree of branching. The MW of the copolymers prepared using emulsion polymerization (10^7–10^9 Da) was generally larger than that of copolymers prepared using solution polymerization (4×10^7–10^8 Da). When the amount of cationic monomer was increased from 10 to 55 mol% in solution polymerization, hydrophobic contraction of the core induced formation of more compact C-PAMs. The copolymers prepared using emulsion polymerization formed highly aggregated or supercoil structures owing to increased intermolecular hydrophobic interaction when less cationic monomer was used. However, the MW decreased with increased cationic group content. In addition, C-PAMs larger than ~10^8 Da prepared using the emulsion method were separated by steric/hyperlayer elution mode while those in the 10^7–10^8 Da range were analyzed in either normal or steric/hyperlayer mode depending on the decay patterns of field programming. Moreover, branched copolymers were found to be resolved with different elution modes under the same field decay pattern depending on the degree of branching: steric/hyperlayer for low-branching and normal for high-branching C-PAMs.

1. Introduction

Cationic polyacrylamides (C-PAMs) are water-soluble copolymers that have polyelectrolyte-like properties owing to the incorporation of cationic groups into the PAM chain [1–3]. Typically, these charged groups are introduced by copolymerizing acrylamide with a vinyl-type cationic monomer having a quaternary ammonium structure such as acryloxyethyltrimethyl ammonium chloride (DAC) [4,5], methacryloxyethyl ammonium chloride (DMC) [6], acryloxyethyl dimethylbenzyl ammonium chloride (AODBAC) [7,8], and etc. Due to the presence of the charged moieties in the macromolecular backbone, C-PAMs have remarkably enhanced properties compared to those of nonionic PAMs for industrial application as flocculants in paper manufacturing and waste water treatment [2,4,9,10]. The improved properties of C-PAMs depend on their molecular weight (MW) and conformation, which is heavily influenced by the density and distribution of positive charge along the polymer chain [2,8]. These parameters are closely related with their flocculation mechanisms in waste water treatments [11]. C-PAM is consisted of two monomers of acrylamide and acryloxyethyltrimethyl ammonium chloride (DAC) as comonomers and when their structures are combined covalently, they form hydrophobic carbon backbone and hydrophilic quaternary ammonium functional group, which is positively charged. C-PAM copolymers synthesized by solution polymerization form hydrophobic cores containing the acrylic monomers and hydrophilic outer shells bearing the carbonyl groups of the cationic monomers [12]. Since the cationic comonomer provides hydrogen bonding with water molecules and induces the hydrophobic contraction of core structures, the copolymers become more compact with increased cationic comonomer content [12]. Moreover, incorporation of branched structures to

* Corresponding author.
E-mail addresses: mhmoon@yonsei.ac.kr, mhmoon@hotmail.com (M.H. Moon).

http://dx.doi.org/10.1016/j.chroma.2017.04.057
0021-9673/

Table 1
List of C-PAM copolymer samples analyzed by FIAF4-MALS-RI system. L, B, and *h*B in the sample ID represent linear, branched, and highly branched structures, respectively.

ID	Structure	Polym. method	Amount of cationic monomer (mol%)	dn/dc	Decay Pattern[a]
LS_{10}	Linear	Solution	10	0.2404	D1
LS_{55}		Solution	55	0.1553	D2
LE_{10}		Emulsion	10	0.1943	D3
LE_{60}		Emulsion	60	0.1707	D4,D5
BS_{10}	Branched	Solution	10	0.2291	D1
BS_{55}		Solution	55	0.0770	D2
BE_{10}		Emulsion	10	0.1074	D2
BE_{40}		Emulsion	40	0.2632	D7
hBE_{40}		Emulsion	40	0.0962	D7
BE_{60}		Emulsion	60	0.1797	D4,D6

D1: 2.0 (4) → 0.83 (3.6) → 0.35 (3.6) → 0.15 (3.6) → 0.07 (3.6) → 0.04 (3.6) → 0.03 (3.6) → 0.02 (3.6).
D2: 2.5 (4) → 1.03 (3.6) → 0.43 (3.6) → 0.19 (3.6) → 0.09 (3.6) → 0.05 (3.6) → 0.03 (3.6) → 0.02 (3.6).
D3. 2.5 (4) → 0.5 (7) → 0.1 (7) → 0.02 (9).
D4: 2.5 (4) → 0.5 (2) → 0.1 (2) → 0.02 (3).
D5: 2.5 (4) → 0.5 (5) → 0.2 (4) → 0.1 (2) → 0.05 (5) → 0.02 (6).
D6: 1.5 (4) → 0.5 (1.33) → 0.1 (2) → 0.02 (2).
D7: 2.5 (4) → 0.5 (2) → 0.2 (1) → 0.1 (2).
[a] Linear decay patterns of crossflow rate in mL/min (elapsed time in min).

these copolymers can improve their properties [13,14], because branched polymers usually have lower viscosities and higher water solubility than linear polymers of the same MW.

Accurate determination of the MWs and molecular conformations of C-PAMs is important for understanding the relationship between polymer materials and their properties and thus to endow materials with desired properties. C-PAM polymers have been characterized by size exclusion chromatography (SEC) [15,16] and intrinsic viscosity measurements [17]. However, C-PAMs with ultrahigh MWs (>10^7 Da) are too large to be analyzed by SEC owing to the lack of analytical columns with suitable pore sizes, and it is extremely difficult to obtain accurate sizes of such large copolymer complexes using intrinsic viscosity measurement [18].

As an alternative separation method to SEC, flow field-flow fractionation with multi-angle light scattering (FlFFF-MALS) has proven capable of size fractionating ultrahigh-MW C-PAMs copolymerized with the cationic monomer DAC, and simultaneously determining MW, MW distribution (MWD), and conformational information for C-PAMs with linear and branched molecular structures [19]. FlFFF is a size-based separation method applicable to macromolecules (both aqueous and organic), nanometer to micron sized particles, and cells [20–23]. Separation in FlFFF takes place in an empty channel space without packing materials by utilizing two perpendicular flow streams: a migration flow moving along the channel that elutes sample components, and a crossflow moving across the channel to drag the migrating sample materials. Size separation in a typical FlFFF system is achieved by the differential migration of sample components depending on their diffusion coefficients, where smaller molecules with faster diffusion protrude further from the channel wall into the higher-velocity streamlines of the migration flow, which exhibits a parabolic velocity pattern, and thus elute faster than larger species (normal elution mode) with slower diffusion. Because FlFFF separation does not rely on the interaction of sample materials with a stationary phase, it can be readily applied to particulate materials or ultrahigh-MW polymers without system blockage. Incorporation of MALS with FlFFF provides accurate MW determination, allowing more precise calculation of average MW (Mw) and MWD and affording structural information on molecular geometry. This technique has been commonly applied to wide variety of polymeric materials, including modified cellulose [24], polysaccharides [25], PAMs [26], amylopectins [27,28], and hyaluronic acids [29–31].

In this study, FlFFF-MALS was utilized to investigate the effect of synthetic parameters on the MWD and molecular structures of a series of ultrahigh-MW C-PAM copolymers, which were prepared by varying the mole fraction of the cationic monomer and the polymerization method (solution vs. emulsion), and also by incorporating branched structures. Elution profiles of the C-PAMs were thoroughly investigated by varying the linear decay patterns of the field strength, i.e., the crossflow rate, in frit inlet asymmetrical FlFFF (FIAF4). While the C-PAM copolymers prepared using solution polymerization were separated in normal elution mode, C-PAMs prepared using emulsion polymerization could be fractionated by both normal and steric/hyperlayer elution modes, in which large molecules elute earlier than smaller ones owing to the negligible contribution of diffusion, depending on the field decay pattern. It was also found that C-PAM samples with similar MWDs can be analyzed in reversed order of size fractionation under the same FlFFF run conditions depending on their branching degree.

2. Experimental

2.1. Materials and reagents

Ten C-PAM copolymer samples, poly(acrylamide-co-*N,N,N*-trimethyl aminoethyl chloride acrylate), were provided by Kolon Life Science Inc. (Gwacheon, Korea) and were synthesized from acrylamide monomers with DAC by two different polymerization methods (solution and emulsion polymerization) with different amounts of DAC and different degree of branching, as listed in Table 1. The C-PAM copolymer samples in powder form were first dissolved at a concentration of 0.5 mg/mL in 0.1 M $NaNO_3$ solution containing 0.02% NaN_3 as a bactericide by stirring with a glass-blade impeller installed in a WiseStir® HS-30E model stirrer from Daihan Scientific Co. (Wonju, Korea) at 300 rpm for 2 h and then at 150 rpm for 22 h. The 0.1 M $NaNO_3$ solution was the carrier solution for FIAF4 analysis, and was prepared with deionized water (>18 MΩ) and filtered with a Durapore® polyvinylidene fluoride membrane filter (pore size 0.1 μm) from Merck Millipore (Darmstadt, Germany) prior to FIAF4-MALS analysis.

2.2. FIAF4-MALS

A model LC Eclipse® channel from Wyatt Technology Europe GmbH (Dernbach, Germany) was utilized to make a frit inlet asymmetrical channel by replacing the plastic inlay used for the depletion wall with a home-made polycarbonate inlay embedded with a ceramic inlet frit (35 mm × 18 mm × 7 mm) at the inlet end of channel. The FIAF4 channel space for separation had the following dimensions: 26.5 cm long, 250 μm thick, 1.6 cm wide at inlet, 0.4 cm wide at outlet, cut from a Mylar sheet. The channel membrane installed was made from regenerated cellulose (MWCO

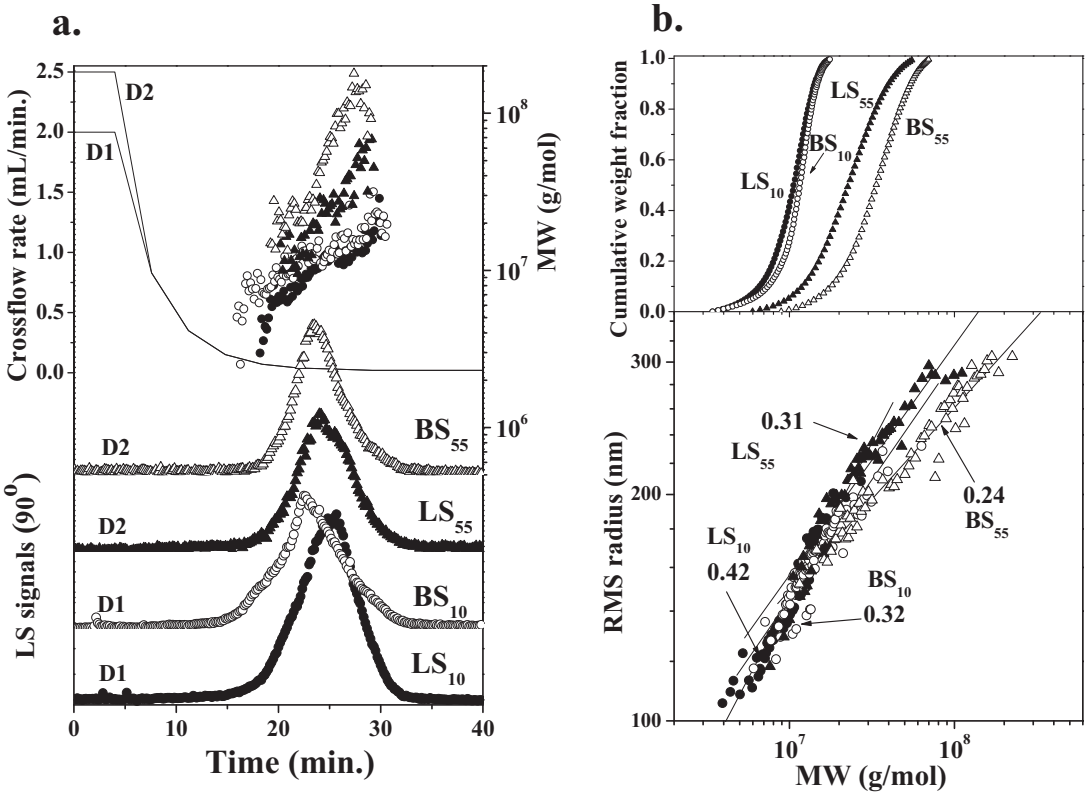

Fig. 1. a) Fractograms (based on LS signals at 90°) and calculated MW values at each time point (top) of C-PAM copolymers prepared from solution polymerization with (BS) and without (LS) branched structures at different comonomer compositions (10 and 55 mol%) under two different linear decay programs (D1 and D2) for FIFA4 separation, and b) the cumulative MWD curves (top) and the conformation plots (bottom) of RMS radius vs. MW of C-PAM samples.

20,000 Da) from Millipore. The carrier solution was delivered to the channel inlet for sample flow and to the inlet frit for frit flow. Sample injection was performed using a model 7725i loop injector from Rheodyne (Cotati, CA, USA), which was installed between a model SP930 HPLC pump from Young-Lin Co. (Seoul, Korea) and the channel inlet. For delivery of frit flow, a model 1260 Infinity HPLC pump from Agilent Technologies (Palo Alto, CA, USA) was utilized. The rates of frit flow, crossflow, and outflow were controlled by an Eclipse system from Wyatt Technology Europe GmbH. Each pump flow (sample flow and frit flow, both immediately after each pump) was filtered again with a PEEK inline filter unit fitted with a PVDF membrane filter with 0.1 μm pores from Wyatt Technology Europe GmbH. Detection of C-PAM materials was performed with a DAWN-DSP MALS at a wavelength of 632.8 nm and a differential refractive index (DRI) of 658 nm with an Optilab T-rEX detector (both from Wyatt Technology, Santa Barbara, CA, USA). Detector signals were recorded with ASTRA software from Wyatt, which was also used for correction of the baseline drift in the fractograms caused by variation in the DRI signals during the decay of the crossflow rate. For baseline correction, a blank run measured before or after each sample run was subtracted from the sample run. Calculation of the C-PAM MW was performed from the MALS signals for detector angles 38.0°, 44.0°, 50.0°, 57.0°, 64.0°, 72.0°, and 81.0° with the dn/dc values measured for each sample (listed in Table 1) utilizing a second-order polynomial fit based on the Berry method of the Debye plot. The dn/dc value was calculated from the DRI signals of sample solutions at six different concentrations by sequentially injecting the diluted samples into the Optilab T-rEX DRI detector.

Injection volume for each C-PAM sample was 10 μg and sample injection was performed at $\dot{V}_s$ = 0.1 mL/min throughout the runs which was identical to the outflow rate, $\dot{V}_{out}$. The crossflow rate, $\dot{V}_c$, was set to be the same as the frit flow rate, $\dot{V}_f$, so that crossflow would decay simultaneously with frit flow decrease. For the programming of field strength, the decay of the crossflow rate was performed linearly with different decay patterns. Several decay patterns were utilized for C-PAM samples in this study, and they are listed in Table 1. For instance, the decay pattern 1 in Table 1 shows that crossflow was maintained at 2.0 mL/min for 4 min at the beginning and decreased linearly to 0.83 mL/min over 3.6 min, further to 0.35 mL/min over 3.6 min, to 0.15 mL/min over 3.6 min, to 0.07 mL/min over 3.6 min, to 0.04 mL/min over 3.6 min, to 0.03 mL/min over 3.6 min, and finally to 0.02 mL/min over 3.6 min, where it was maintained until the end of the run.

3. Results and discussion

The C-PAM copolymers examined in this study were prepared with different cationic comonomer contents (mol%) and either with or without branched structures using both solution and emulsion polymerization methods. Consequently, run conditions were selected depending on the nature of the copolymer sample by varying the field decay patterns (see Table 1) in FIAF4. Fig. 1a shows the fractograms (based on MALS signals at 90°) of the four C-PAM copolymers that were prepared by the solution polymerization method (indicated by an S in the sample label) with different DAC comonomer contents (10 and 55 mol%) and linear (L) or branched (B) copolymer structures, along with the calculated MW data points (top of Fig. 1a) at each time point. The same type of symbol was used to represent both the fractogram and the corresponding MW data points for each sample. The plots of D1 and D2 at the top of Fig. 1a represent the decay patterns for the crossflow rate that were employed for the separation of samples with 10 and 55 mol% cationic monomer contents, respectively. Separation in

Table 2
Calculated Mw (weight average molecular weight), Mn (number average molecular weight), polydispersity (Mw/Mn), Rw (weight average RMS radius), Rn (number average RMS radius), and slope of RMS radius plot (versus MW) for the C-PAM samples.

Sample ID	Mw (g/mol)	Mn (g/mol)	Polydispersity	Rw (nm)	Rn (nm)	Slope
LS_{10}	$(1.09 \pm 0.66) \times 10^7$	$(9.64 \pm 0.07) \times 10^6$	1.08 ± 0.03	150.9 ± 4.9	142.5 ± 4.8	0.42 ± 0.00
LS_{55}	$(2.01 \pm 0.14) \times 10^7$	$(1.70 \pm 0.19) \times 10^7$	1.19 ± 0.05	200.5 ± 5.6	191.1 ± 4.3	0.31 ± 0.00
BS_{10}	$(1.17 \pm 0.05) \times 10^7$	$(1.10 \pm 0.09) \times 10^7$	1.18 ± 0.03	158.0 ± 1.8	155.2 ± 0.6	0.32 ± 0.01
BS_{55}	$(3.68 \pm 0.27) \times 10^7$	$(2.94 \pm 0.03) \times 10^7$	1.28 ± 0.09	217.7 ± 4.5	205.4 ± 4.6	0.24 ± 0.01
LE_{10}	$(2.65 \pm 0.27) \times 10^8$	$(1.13 \pm 0.39) \times 10^8$	2.38 ± 0.17	448.9 ± 3.9	365.2 ± 3.3	0.12 ± 0.01, 0.36 ± 0.01
LE_{60}	$(2.50 \pm 0.53) \times 10^7$	$(2.00 \pm 0.37) \times 10^7$	1.21 ± 0.04	227.6 ± 13.9	211.1 ± 7.7	0.33 ± 0.02
BE_{10}	$(4.73 \pm 0.34) \times 10^8$	$(1.09 \pm 0.66) \times 10^8$	1.34 ± 0.05	501.0 ± 1.1	466.6 ± 2.8	0.15 ± 0.01, 0.35 ± 0.01
BE_{40}	$(5.29 \pm 0.53) \times 10^7$	$(3.37 \pm 0.83) \times 10^7$	1.41 ± 0.19	273.0 ± 2.1	238.8 ± 14.8	0.42 ± 0.01
hBE$_{40}$	$(5.00 \pm 0.01) \times 10^7$	$(3.90 \pm 0.00) \times 10^7$	1.28 ± 0.04	230.9 ± 0.6	216.8 ± 0.6	0.24 ± 0.04
BE_{60}	$(3.72 \pm 0.84) \times 10^7$	$(2.52 \pm 0.34) \times 10^7$	1.51 ± 0.59	263.8 ± 12.8	242.6 ± 3.5	0.26 ± 0.00

FIAF4 is achieved continuously by hydrodynamic relaxation without employing the typical focusing/relaxation method that halts sample migration for a certain period of time. In hydrodynamic relaxation, sample components injected into the FIAF4 channel achieve equilibrium between the driving forces of crossflow movement across the channel and diffusion against the channel wall through the compressive action of the high frit flow to the incoming sample components while they migrate along the channel. When utilizing field-programmed separation in FIAF4, the successful relaxation of sample components must be assured during injection by providing a suitable initial field strength and decay pattern. Incomplete relaxation often causes a perturbation in size based elution of sample components, especially in the beginning of elution. For the samples prepared with a 10 mol% cationic monomer content (LS_{10} and BS_{10}), the data points at the top of Fig. 1a show gradual increases in MW with retention time without significant perturbation in the early stages of elution. In cases of incomplete relaxation, the MW values at the beginning of the elution are scattered and do not increase smoothly with time. Thus, the retentions for LS_{10} and BS_{10} are suitable for run condition D1. In the case of BS_{10}, which contains branched molecules, the calculated MW value appears to be slightly larger than that for linear molecules at the same retention time. This results from the fact that branched molecules have more compact geometries than their linear counterparts. This results in a decrease in elution time because FlFFF separation relies on the hydrodynamic diameter of macromolecules. This is clearly demonstrated by the shift of the fractogram for BS_{10} to a shorter time scale compared to that of LS_{10}, while their MWD curves are similar (top panel of Fig. 1b). The difference in the molecular structures of the two samples is further indicated by the difference in the slope values of their conformation plots (root mean square (RMS) radius vs. MW), which are 0.42 for the linear (LS_{10}) and 0.32 for the branched (BS_{10}) C-PAM samples (bottom panel of Fig. 1b). However, the two samples with the higher cationic comonomer content (55 mol%) needed to be run with decay pattern D2, which has a higher initial field strength (2.5 mL/min) that is required for larger MW species to reach equilibrium heights closer to the channel wall. Initial field strength of 2.0 mL/min from decay pattern D1 was not strong enough for much larger C-PAM molecules of both LS_{55} and BS_{55} to reach their equilibrium positions, which resulted in perturbation in the elution of large MW species (not shown here). Therefore, the decay pattern D2 with a higher initial field strength was utilized for samples with the higher cationic comonomer content. By comparing the calculated MW data points (filled triangles for LS_{55} and open triangles for BS_{55}) in the top two plots in Fig. 1a, the MW of the branched sample (BS_{55}, open triangles) increases more rapidly with increasing time than that of the linear sample (filled triangles), indicating that branched molecules above $\sim 2 \times 10^7$ Da are much more compact in their geometries than their linear counterparts. This can be confirmed from the calculated slope values of the conformation plots in Fig. 1b, which are 0.31 for LS_{55} and 0.24 for BS_{55}. The further decrease in slope value below ~0.3 is likely to be caused by the formation of entangled network structures in the ultrahigh MW region. The MWD of C-PAM significantly increases with increasing cationic comonomer content (both for LS_{55} and BS_{55}) and Mw increases approximately two- to three-fold, as shown in Table 2 55 mol% samples decrease with increasing cationic monomer content (from 0.42 to 0.31 for the LS sample and from 0.32 to 0.24 for the BS samples). During the solution polymerization of C-PAMs, it is likely that polyacrylamide chains form hydrophobic cores while hydrophilic cationic monomers are located on the outer shell and interact with water molecules by hydrogen bonding, resulting in stronger interaction with surrounding water molecules. Therefore, an increase in cationic comonomer content is thought to induce more compact packing geometries.

Similar comparisons were made for C-PAMs prepared by emulsion polymerization (indicated by an E in the sample label), as shown in Fig. 2. However, a diverse range of field decay patterns were required to run the extremely large MW copolymers with either linear or branched structures prepared using 10 and 60 mol% cationic monomer contents. Noticeably, C-PAMs prepared using the emulsion polymerization method appear to be much larger (10^7–10^9 Da, shown in the MW plots in Fig. 2a) than those prepared using solution polymerization (4×10^6–10^8 Da). Moreover, in steric/hyperlayer elution mode, of which elution order is opposite to that in normal mode (as observed in Fig. 1), the large-MW C-PAMs prepared using emulsion polymerization elute first without significant perturbation at the beginning of the elution, especially the extremely large molecules (>10^9 Da). The range of RMS radius values for C-PAMs prepared using emulsion polymerization (200–700 nm in Fig. 2b) is much larger than that (100–300 nm) of C-PAMs prepared using solution polymerization. This indicates that C-PAMs prepared using emulsion polymerization are sufficiently large enough to be resolved in steric/hyperlayer elution mode. The two C-PAMs prepared with a cationic monomer content of 10 mol% (LE_{10} and BE_{10}) needed to be run with slightly different decay patterns (D3 and D2, respectively) and the elution order observed from the calculated MW data points in the top panel of Fig. 2a is clearly of the steric/hyperlayer separation. The other two C-PAMs with cationic monomer contents of 60 mol% (LE_{60} and BE_{60}) were not resolved under either D2 or D3 conditions and needed to be resolved with the faster field decay pattern D4. A faster field decay was required to elute high-retention highly ionic C-PAM molecules (smaller sizes in steric/hyperlayer elution) since the hydrodynamic lift forces of these molecules (LE_{60} and BE_{60}) are weaker than those applied to the relatively bulky C-PAMs (LE_{10} and BE_{10}) prepared with lower cationic monomer contents. The difference in size can be confirmed in the conformation plot shown in Fig. 2b. The RMS radius values for BE_{10} at all MW values are smaller than those for

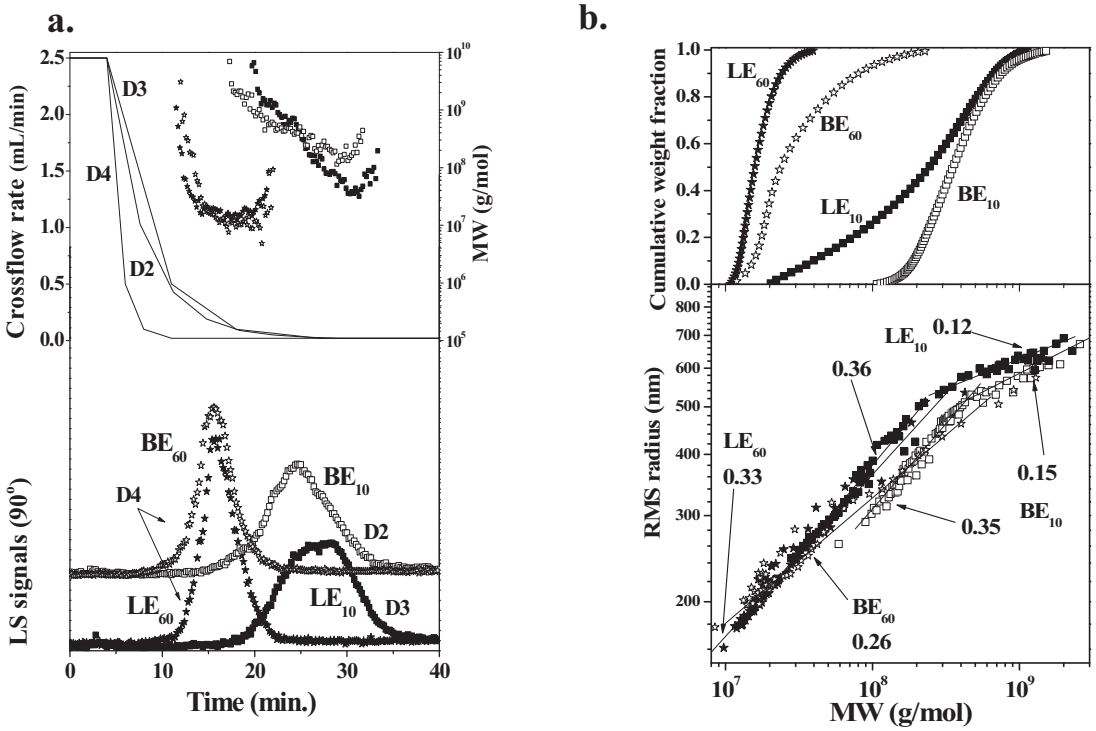

Fig. 2. a) Fractograms (bottom) and calculated MW values (top) of C-PAMs prepared using emulsion polymerization with (BE) and without (LE) branched structures at different comonomer compositions (10 and 60 mol%), and b) the cumulative MWD curves (top) conformation plots for C-PAMs.

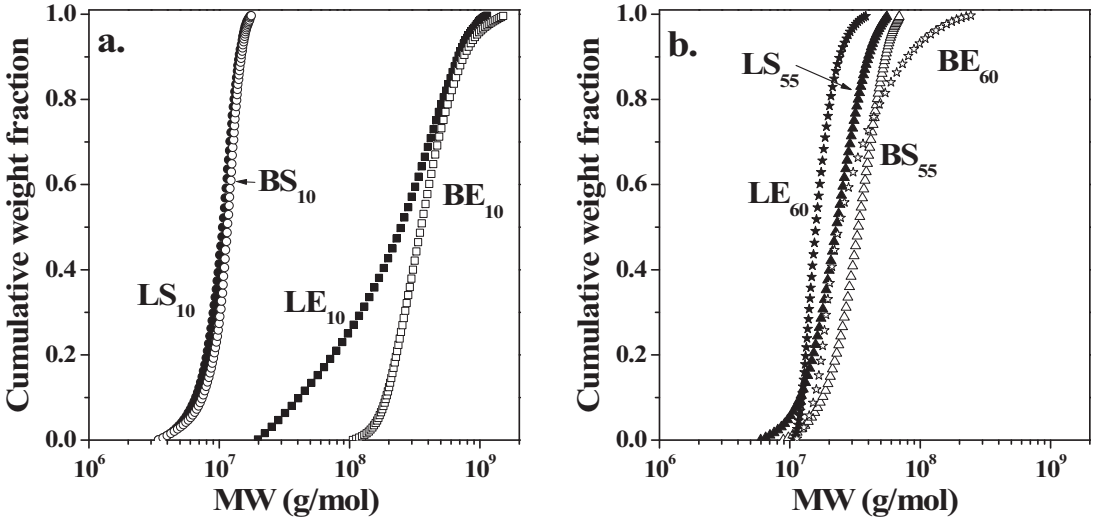

Fig. 3. Superimposed MWD curves representing the effect of branching on the MWDs of C-PAMs prepared with cationic copolymer contents of a) 10 mol% and b) 55 and 60 mol%.

LE_{10}, which is caused by the branching effect. However, the difference in size between LE_{60} and $BE_{60}$is not significant, indicating that the shrinking of molecular structure with increased cationic monomer content is not significant in the emulsion polymerization method but is significant in solution polymerization (see Fig. 1b). Moreover, comparison of the conformation plots shows that less ionic C-PAMs (LE_{10} and BE_{10}) have two different slope values for their RMS radius plots, 0.35–0.36 and 0.12–0.15, respectively, indicating that these samples are present in different conformations. Each of the conformation plots is separately plotted in Fig. S1 for clear comparison of the effect of ionic content within the linear and branched structures. Fig. S1a shows the conformation plots of both linear C-PAMs (LE_{10} and LE_{60}). The slope values for the linear copolymers smaller than $\sim 3 \times 10^8$ Da are similar (0.36 and 0.33, respectively), indicating spherical structures, while the slope value for those larger than $\sim 3 \times 10^8$ Da is 0.12, which indicates highly aggregated or supercoiled structures. The extremely large MW region ($>\sim 3 \times 10^8$ Da) is found only with less ionic C-PAM samples prepared by the emulsion method. This phenomenon is also observed for the branched molecules, as indicated by the low slope value (0.15 for BE_{10}) in the extremely large MW regime. However, the slope value for BE_{60} further decreases to 0.26. For these experiments, it can be summarized that highly aggregated structures with extremely large MWs ($\sim 3 \times 10^8$–10^9 Da) appear at low ionic contents (10 mol%), while those aggregates disappear with increasing ionic content (60 mol%). Fig. 3 compares the MWDs of C-

PAM molecules with linear and branched structures and the same cationic comonomer content. C-PAM copolymers with low ionic contents prepared using emulsion polymerization are one order of magnitude larger in terms of Mw and exhibit broader MWDs than those prepared using solution polymerization, as shown in Fig. 3a. However, C-PAMs with high ionic contents are similar in their MWDs, as shown in Fig. 3b.

While most C-PAMs prepared using emulsion polymerization are resolved by FIAF4 in steric/hyperlayer mode, as shown in Fig. 2a, LE_{60} and BE_{60} samples appear with a distinct reversal of elution order at the end of the run. These samples were further investigated by varying the decay period for successful fractionation under normal mode, and the results for LE_{60} are shown in Fig. 4 (BE_{60} results are presented in Fig. S2). During hydrodynamic relaxation, ultrahigh-MW species larger than $\sim 10^8$ Da may experience strong hydrodynamic lift forces so that they can elute in steric/hyperlayer mode [19]. However, when the field strength begins to decay, migrating polymer molecules of smaller sizes experience secondary relaxation to adjust their equilibrium heights upward from the channel wall. When the field further decreases to the level where the lift force contribution becomes negligible compared to diffusional forces, then sample components follow the normal mode of elution. This is clearly demonstrated with the LE_{60} sample by varying the decay pattern. Fig. 4a and b are the fractograms of LE_{60} obtained under D4 and D5, respectively, and species eluted in steric/hyperlayer mode are marked with filled symbols while those eluted in normal mode are marked with open symbols. With the fast decay pattern D4, most molecules elute in steric/hyperlayer mode, as seen by comparing the peak area of the two regimes in the fractogram (panel a), which are divided by the vertical dashed line marked for steric inversion. However, under the delayed decay pattern D5, copolymer molecules that migrate slowly at the beginning of separation experience reduced lift forces during field decay and achieve a secondary equilibrium dominated by molecular diffusion. Therefore, most LE_{60} copolymer molecules elute in normal mode (open triangles in panel b). From the MWD curve of LE_{60} in Fig. 2b, two parallel dotted lines at 10^7 and 10^8 Da are inserted in Fig. 4 as boundaries of the MWD. Most LE_{60} molecules are readily resolved by either steric/hyperlayer or normal modes without significant perturbation in the elution. Calculated Mw values for LE_{60} from the two different run conditions are 2.50×10^7 from decay pattern D4 and 2.55×10^7 from D5, as shown in Table S1, which are very similar. In Fig. 4c, RMS radius plots with different symbols are superimposed, showing circles for D4 and triangles for D5, as well as steric/hyperlayer elution (filled symbols) and normal elution (open symbols). It is likely that polymer molecules that are larger than 10^8 Da and elute in steric/hyperlayer mode (upper left of the MW plots in Fig. 4a and b) appear at much larger RMS radius values (filled circles and filled triangles in panel c) than those (open symbols) that belong to the linear clusters of data points. These outliers may be exceptionally bulky molecules, or may be caused by errors in the calculation of MW and RMS radius values due to the weak signal intensity at the beginning of elution. However, their contribution to the entire MWD is negligible due to their low concentrations.

Similar experiments were performed with BE_{60}, but the comparison was made using the low initial field strength adopted for the normal mode of separation, as shown in Fig. S2. In order to reduce the hydrodynamic lift forces for ultrahigh-MW species larger than 10^8 Da in the BE_{60} sample, the initial field strength was lowered to 1.5 mL/min for decay pattern D6, under which most of the copolymers experience weak lift forces and thus elute in normal mode (Fig. S2b). In Fig. S2b, ultrahigh-MW species ($> 3 \times 10^8$ Da) are rarely detected under these run conditions, perhaps due to poor resolution during steric/hyperlayer elution due to insufficient lift forces.

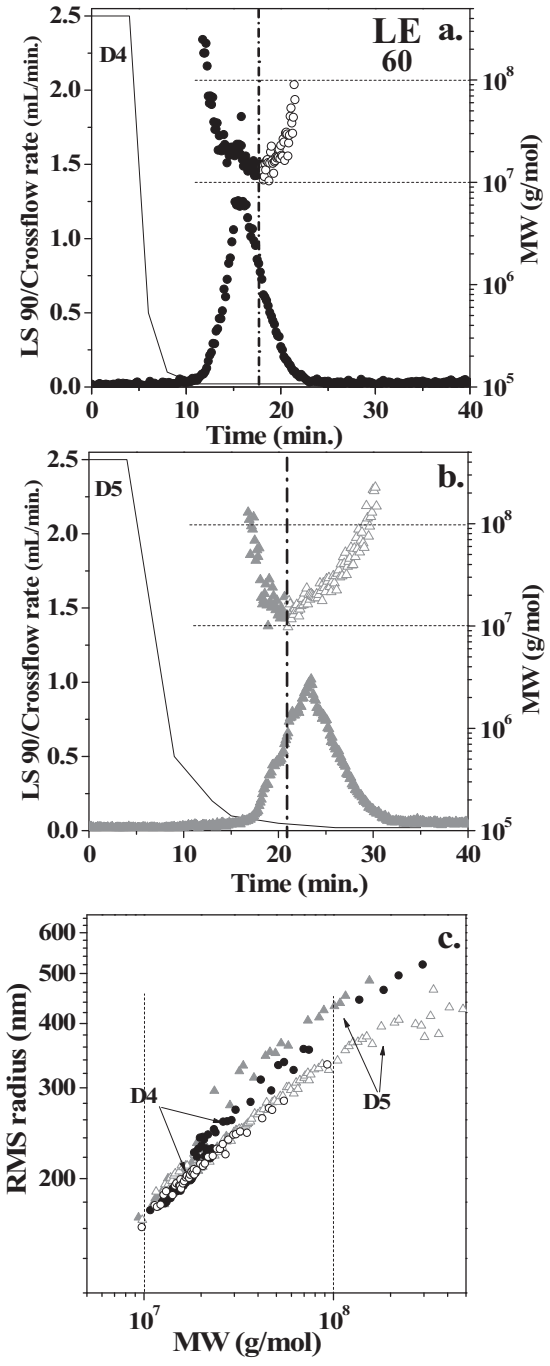

Fig. 4. Conversion of the elution modes. a) Steric/hyperlayer mode and b) the normal mode, observed with LE_{60} C-PAM molecules by FIAF4 depending on the linear decay patterns of crossflow rate (D4 and D5), respectively, and c) a comparison of RMS radius plots. Symbols in plot 'c' match with the type of symbols used in the calculated MW data that are marked differently depending on the elution mode: filled symbols (circles and triangles) for steric/hyperlayer elution and open symbols for normal mode.

This results in a difference in Mw values for BE_{60}, i.e., 3.72×10^7 for decay pattern D4 and 2.42×10^7 for D6 (Table S1).

Finally, the branching degree of the C-PAMs can alter their elution pattern between steric/hyperlayer and normal modes under the same FIAF4 run conditions. For C-PAM samples prepared using emulsion polymerization with an ionic comonomer content of 40 mol% with differing branching degrees, i.e., BE_{40} and hBE_{40} (where *h* indicates highly branched), the samples show opposite orders of elution under the same FIAF4 flow rate conditions (D7,

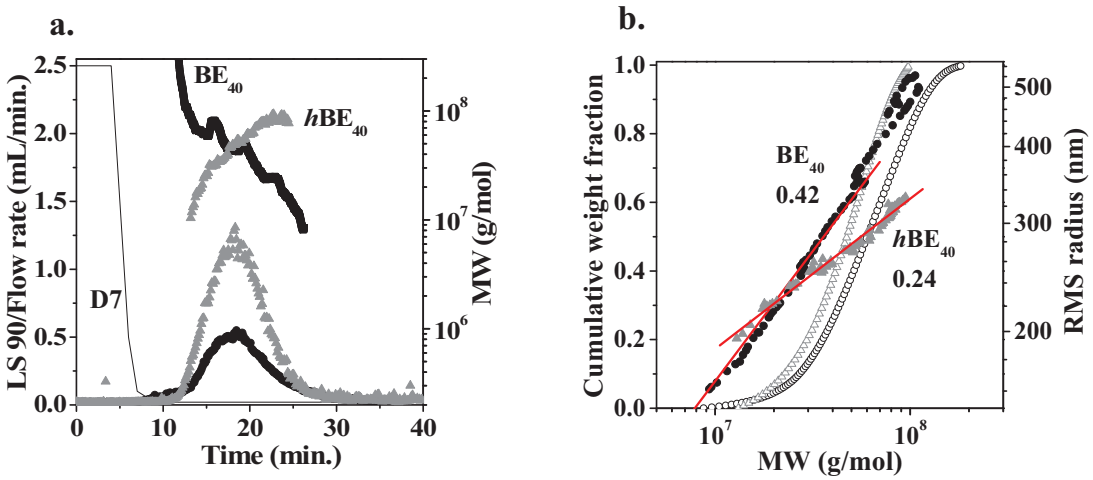

Fig. 5. Effect of branching degree in an emulsion polymerized C-PAM sample (BE_{40}) on the elution pattern in FIAF4 obtained under the same flowrate conditions: a) Fractograms of BE_{40} and hBE_{40} molecules, and b) conformational plots showing the significant differences in geometrical structures of the two branched copolymers.

which is slightly different from D4), as shown in Fig. 5. The branching degree of hBE_{40} was 2.5 times higher than that of BE_{40} of which branching degree is the same as all the branched samples examined in this study. As expected from the results for BE_{10} and BE_{60}, separation of BE_{40} is achieved in steric/hyperlayer mode, as shown in Fig. 5a. However, highly branched hBE_{40} is resolved in the opposite order of elution for normal mode. The MWDs for both BE40 and hBE_{40} are similar (10^7–10^8 Da in Fig. 5b) but there is a clear difference in the conformation of the copolymers, as indicated by the different slope values of the RMS radius plots, i.e., 0.42 and 0.24 for BE40 and hBE_{40}, respectively. The calculated Mw and Rw (i.e., the average RMS radius) values in Table 2 indicate that highly branched molecules are much more compact in geometry even though they have similar Mw values. Although the conformation of BE_{10} is 0.35 (Fig. 2b) which is rather spherical in geometry, the MW range of BE_{10} is very large (>10^8 Da), and therefore it was separated in steric/hyperlayer mode. However, an increase in branching degree is expected to lead to more compact geometry than that in less branched molecules, but it may reduce the lift force contribution of molecules in the intermediate MW range (10^7–10^8 Da), and thus lead to these molecules eluting in normal mode in FIAF4.

4. Conclusion

This study utilized FIAF4-MALS to obtain MWD and conformation information for C-PAM copolymers with varying cationic monomer contents prepared using both solution and emulsion polymerization methods. For C-PAMs prepared from solution polymerization, the Mw increases and molecular conformation becomes more compact with increased ionic monomer content (from 10 to 60 mol%) regardless of branching structure. However, the opposite trend is observed for C-PAMs prepared using emulsion polymerization, i.e., C-PAMs with lower ionic charge have much larger Mw values along with highly aggregated structures ($\sim 3 \times 10^8$–10^9 Da), and their MWs decrease along with the disappearance of aggregates with increasing cationic content. These trends were observed for both linear and branched molecules. In emulsion polymerization, the shrinkage of molecular structure by the branching effect is significant in C-PAMs with fewer ionic groups, but not for those with a larger amount of ionic groups. However, this shrinkage is significant in higher ionic C-PAMs prepared using solution polymerization.

During the analysis of ultrahigh-MW C-PAM molecules by field programmed separation in FIAF4, it was observed that all the linear and branched C-PAM samples prepared by solution method were less than $\sim 2 \times 10^8$ Da and readily resolved under normal separation mode. However, C-PAMs larger than $\sim 10^8$ Da prepared by the emulsion method were separated by steric/hyperlayer elution mode. The calculated RMS radius values observed for 10^8 Da polymers corresponded to ~300 nm for branched and ~400 nm for linear C-PAMs, based on the results of BE_{10} and LE_{10}, respectively. This demonstrates that C-PAMs in the 10^7–10^8 Da range prepared by the emulsion method can be analyzed in either normal or steric/hyperlayer mode by varying the initial field strength or field decay pattern, because C-PAMs prepared using the emulsion method are more bulky than those prepared using the solution method. During hydrodynamic relaxation in FIAF4 separation, extremely large molecules can experience lift forces that are significantly larger than the diffusional contribution, and therefore they quickly elute in steric/hyperlayer mode. However, large molecules in the intermediate MW range or with MWs around the steric inversion point elute slowly at the beginning of run and they may experience secondary relaxation when the field strength decays. In extreme cases, they follow a normal mode of retention when the field strength decays to a level where the lift force contribution is negligible. Moreover, we demonstrated that C-PAMs with different degrees of branching but similar MWDs can be oppositely resolved with the same field decay program depending on the degree of branching, i.e., steric/hyperlayer mode for C-PAMs with lower degree of branching and normal mode for highly branched samples.

Acknowledgement

This study was supported by a grant (2015R1A2A1A01004677) from the National Research Foundation of Korea.

Appendix A. Supplementary data

Supplementary data associated with this article can be found, in the online version, at http://dx.doi.org/10.1016/j.chroma.2017.04.057.

References

[1] W. Jaeger, J. Bohrisch, A. Laschewsky, Synthetic polymers with quaternary nitrogen atoms—synthesis and structure of the most used type of cationic polyelectrolytes, Prog. Polym. Sci. 35 (2010) 511–577.

[2] E. Antunes, F.A.P. Garcia, P. Ferreira, A. Blanco, C. Negro, M.G. Rasteiro, Use of new branched cationic polyacrylamides to improve retention and drainage in papermaking, Ind. Eng. Chem. Res. 47 (2008) 9370–9375.
[3] K.A. Klimchuk, M.B. Hocking, S. Lowen, Water-soluble acrylamide copolymers. IX. Preparation and characterization of the cationic derivatives of poly (acrylamide-co-n, n-dimethylacrylamide), poly (acrylamide-co-methacrylamide), and poly (acrylamide-co-n-t-butylacrylamide), J. Polym. Sci. A: Polym. Chem. 39 (2001) 2525–2535.
[4] W. Sun, G. Zhang, L. Pan, H. Li, A. Shi, Synthesis, characterization, flocculation properties of branched cationic polyacrylamide, Int. J. Polym. Sci. 2013 (2013) (Article ID 397027).
[5] F. Mabire, R. Audebert, C. Quivoron, Synthesis and solution properties of water soluble copolymers based on acrylamide and quaternary ammonium acrylic comonomer, Polymer 25 (1984) 1317–1322.
[6] D. Chen, Z. Liu, Y. Yue, W. Zhang, P. Wang, Dispersion copolymerization of acrylamide with quaternary ammonium cationic monomer in aqueous salt solution, Eur. Polym. J. 42 (2006) 1284–1297.
[7] M.S. Cho, B.K. Song, K.J. Yoon, Flocculation characteristics of copolymer of acrylamide with quaternary ammonium cationic monomer (running) flocculation by cationic polyacrylamide, J. Ind. Eng. Chem. 8 (2002) 131–137.
[8] B.K. Song, M.S. Cho, K.J. Yoon, D.C. Lee, Dispersion polymerization of acrylamide with quaternary ammonium cationic comonomer in aqueous solution, J. Appl. Polym. Sci. 87 (2003) 1101–1108.
[9] R. Nicke, S. Pensold, H.-J. Hartman, M. Tappe, Polysiallyldimethylammonium chloride as a flocculating agent, Wochenbl. Paperfabr. 120 (1992) 559–564.
[10] M. Smollen, Dewaterability of municipal sludge 1: a comparative study of specific resistance to filtration and capillary suction time as dewaterability parameters, Water SA 12 (1986) 127–132.
[11] C.S. Lee, J. Robinson, M.F. Chong, A review on application of flocculants in wastewater treatment, Process. Saf. Environ. Prot. 92 (2014) 489–508.
[12] R. Losada, C. Wandrey, Copolymerization of a cationic double-charged monomer and electrochemical properties of the copolymers, Macromolecules 42 (2009) 3285–3293.
[13] I.J. Hobson, W.J. Feast, Polyamidoamine hyperbranched systems: synthesis, structure and characterization, Polymer 40 (1999) 1279–1297.
[14] J.-H. Shin, S.H. Han, C. Sohn, S.K. Ow, S. Mah, Highly branched cationic polyelectrolytes: filler flocculation, Tappi. J. 80 (1997) 179–185.
[15] M.S. Cho, B.K. Song, K.J. Yoon, Flocculation characteristics of copolymer of acrylamide with quaternary ammonium cationic monomer (running) flocculation by cationic polyacrylamide, J. Ind. Eng. Chem. 8 (2002) 131–137.
[16] B.K. Song, M.S. Cho, K.J. Yoon, D.C. Lee, Dispersion polymerization of acrylamide with quaternary ammonium cationic comonomer in aqueous solution, J. Appl. Polym. Sci. 87 (2003) 1101–1108.
[17] F. Mabire, R. Audebert, C. Quivoron, Synthesis and solution properties of water soluble copolymers based on acrylamide and quaternary ammonium acrylic comonomer, Polymer 25 (1984) 1317–1322.
[18] E. Antunes, F.A.P. Garcia, P. Ferreira, A. Blanco, C. Negro, M.G. Rasteiro, Use of new branched cationic polyacrylamides to improve retention and drainage in papermaking, Ind. Eng. Chem. Res. 47 (2008) 9370–9375.
[19] S. Woo, J.Y. Lee, W. Choi, M.H. Moon, Characterization of ultrahigh molecular weight cationic polyacrylamide by frit-inlet asymmetrical flow field-flow fractionation and multiangle lightscattering, J. Chromatogr. A 1429 (2016) 304–310.
[20] J.C. Giddings, Field-flow fractionation: analysis of macromolecular, colloidal, and particulate materials, Science 260 (1993) 1456–1465.
[21] M.E. Schimpf, K.D. Caldwell, J.C. Giddings, Field-Flow Fractionation Handbook, Wiley Interscience, New York, 2000.
[22] K.-G. Wahlund, J.C. Giddings, Properties of an asymmetrical flow field-flow fractionation channel having one permeable wall, Anal. Chem. 59 (1987) 1332–1339.
[23] S.K. Ratanathanawongs, J.C. Giddings, Dual-field and flow-programmed lift hyperlayer field-flow fractionation, Anal. Chem. 64 (1992) 6–15.
[24] M. Andersson, B. Wittgren, H. Schagerlof, D. Momcilovic, K.G. Wahlund, Size and structure characterization of ethylhydroxyethyl cellulose by the combination of field-flow fractionation with other techniques. Investigation of ultralarge components, Biomacromolecules 5 (2004) 97–105.
[25] B. Wittgren, K.-G. Wahlund, Fast molecular mass and size characterization of polysaccharides using asymmetrical flow field-flow fractionation-multiangle light scattering, J. Chromatogr. A 760 (1997) 205–218.
[26] R. Hecker, P.D. Fawell, A. Jefferson, J.B. Farrow, Flow field-flow fractionation of high-molecular-mass polyacrylamide, J. Chromatogr. A 837 (1999) 139–151.
[27] M. Van Bruijinsvoort, K.-G. Wahlund, G. Nilsson, W.T. Kok, Retention behaviour of amylopectins in asymmetrical flow field-flow fractionation studied by multi-angle light scattering detection, J. Chromatogr. A 925 (2001) 171–182.
[28] S. Lee, P.-O. Nilsson, G.S. Nilsson, K.-G. Wahlund, Development of asymmetrical flow field-flow fractionation–multi angle laser light scattering analysis for molecular mass characterization of cationic potato amylopectin, J. Chromatogr. A 1011 (2003) 111–123.
[29] D.Y. Shin, E. Hwang, I.-H. Cho, M.H. Moon, Molecular weight and structure characterization of sodium hyaluronate and its gamma radiation degradation products by flow field-flow fractionation and on-line multiangle light scattering, J. Chromatogr. A 1160 (2007) 270–275.
[30] M.H. Moon, Flow field-flow fractionation and multiangle light scattering for ultrahigh molecular weight sodium hyaluronate characterization, J. Sep. Sci 33 (2010) 3519–3529.
[31] B. Kim, S. Woo, Y.-S. Park, E. Hwang, M.H. Moon, Ionic strength effect on molecular structure of hyaluronic acid investigated by flow field-Flow fractionation and multiangle light scattering, Anal. Bioanal. Chem. 407 (2015) 1327–1334.